ACS Chemical Neuroscience

RESEARCH ARTICLE

pubs.acs.org/acschemicalneuroscience

Biocytin-Derived MRI Contrast Agent for Longitudinal Brain Connectivity Studies

Anurag Mishra,[*,†,⊥] Almut Schüz,[†] Jörn Engelmann,[‡] Michael Beyerlein,[†] Nikos K. Logothetis,[†,§] and Santiago Canals[*,†,∥]

[†]Department for Physiology of Cognitive Processes and [‡]High-Field MR Center, Max-Planck Institute for Biological Cybernetics, Spemannstrasse 38, 72076 Tübingen, Germany

[§]Imaging Science and Biomedical Engineering, University of Manchester, Manchester M13 9PL, England

[∥]Instituto de Neurociencias CSIC-UMH, Campus de San Juan, 03550 San Juan de Alicante, Spain

Supporting Information

ABSTRACT: To investigate the connectivity of brain networks noninvasively and dynamically, we have developed a new strategy to functionalize neuronal tracers and designed a biocompatible probe that can be visualized in vivo using magnetic resonance imaging (MRI). Furthermore, the multimodal design used allows combined ex vivo studies with microscopic spatial resolution by conventional histochemical techniques. We present data on the functionalization of biocytin, a well-known neuronal tract tracer, and demonstrate the validity of the approach by showing brain networks of cortical connectivity in live rats under MRI, together with the corresponding microscopic details, such as fibers and neuronal morphology under light microscopy. We further demonstrate that the developed molecule is the first MRI-visible probe to preferentially trace retrograde connections. Our study offers a new platform for the development of multimodal molecular imaging tools of broad interest in neuroscience, that capture in vivo the dynamics of large scale neural networks together with their microscopic characteristics, thereby spanning several organizational levels.

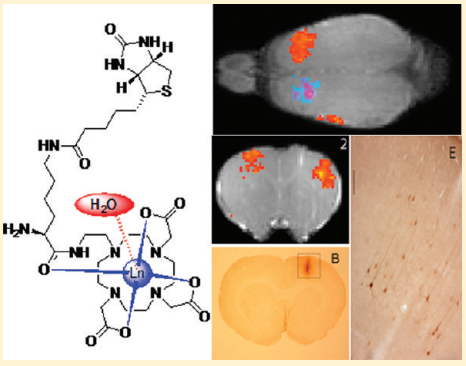

KEYWORDS: Gadolinium, biocytin, imaging probe, neuronal tract-tracing, histology

There is a general consensus in the neuroscientific field on the prime importance of understanding brain connectivity to advance our understanding of brain function and disease.[1,2] In particular, the profuse pattern of connections of the cerebral cortex plays an important role for cognitive functions.[3] Research over the past few years has added additional complexity to the connectivity problem, challenging the view of the brain as a rigid system and demonstrating that it is rather a plastic structure with connections adapting to the environment. For instance, connectivity can change in the course of learning, drug addiction, epilepsy, and other neurodegenerative diseases.[2,4−6] In order to better relate the anatomical structure of the brain to a particular functional outcome and to follow changes with development and aging, longitudinal studies on an individual basis are required. There are not many techniques that give us the opportunity of approaching this goal. For its broad spatial coverage and 3D noninvasive nature, magnetic resonance imaging (MRI) stands as an excellent candidate for dynamic investigations of brain connectivity.

We report here a strategy to produce novel MR contrast agents to dynamically trace brain connectivity in vivo by functionalizing classical neuroanatomical tracer molecules. Classical tracers are taken up by neurons and transported from the soma and dendrites to the distant synaptic terminals (anterograde tracers) or toward the soma (retrograde tracers).[7] These compounds are visualized with conventional histological techniques in post-mortem samples. Thus, the outputs from and inputs to a particular brain area are delineated only after processing of the fixed brain tissue. Previous and successful attempts to investigate neuronal connectivity in vivo using MRI and the paramagnetic ion manganese (Mn^{2+}) have been reported.[8] In manganese-enhanced MRI (MEMRI), Mn^{2+} is taken up by neurons and transported to the distant synaptic terminals where it accumulates and reveals the projection fields.[8−14] Combined anterograde and retrograde transport has also been reported using MEMRI.[15] Also reported is, however, the toxicity associated with high concentration of Mn^{2+} in tissue that challenges the applicability of the MEMRI technique.[10,16,17] Although some strategies have been reported to decrease the impact of Mn^{2+} toxicity on MEMRI experiments,[10,18−20] new nontoxic paramagnetic tracers are desirable.

To develop new neuronal tracers for connectivity studies in living animals, we have focused, as a proof of concept, on the well-known classical tracer biocytin.[21] The backbone of this structure was functionalized by covalently linking the gadolinium (Gd^{3+})

Received: March 7, 2011
Accepted: August 3, 2011
Published: August 03, 2011

Scheme 1[a]

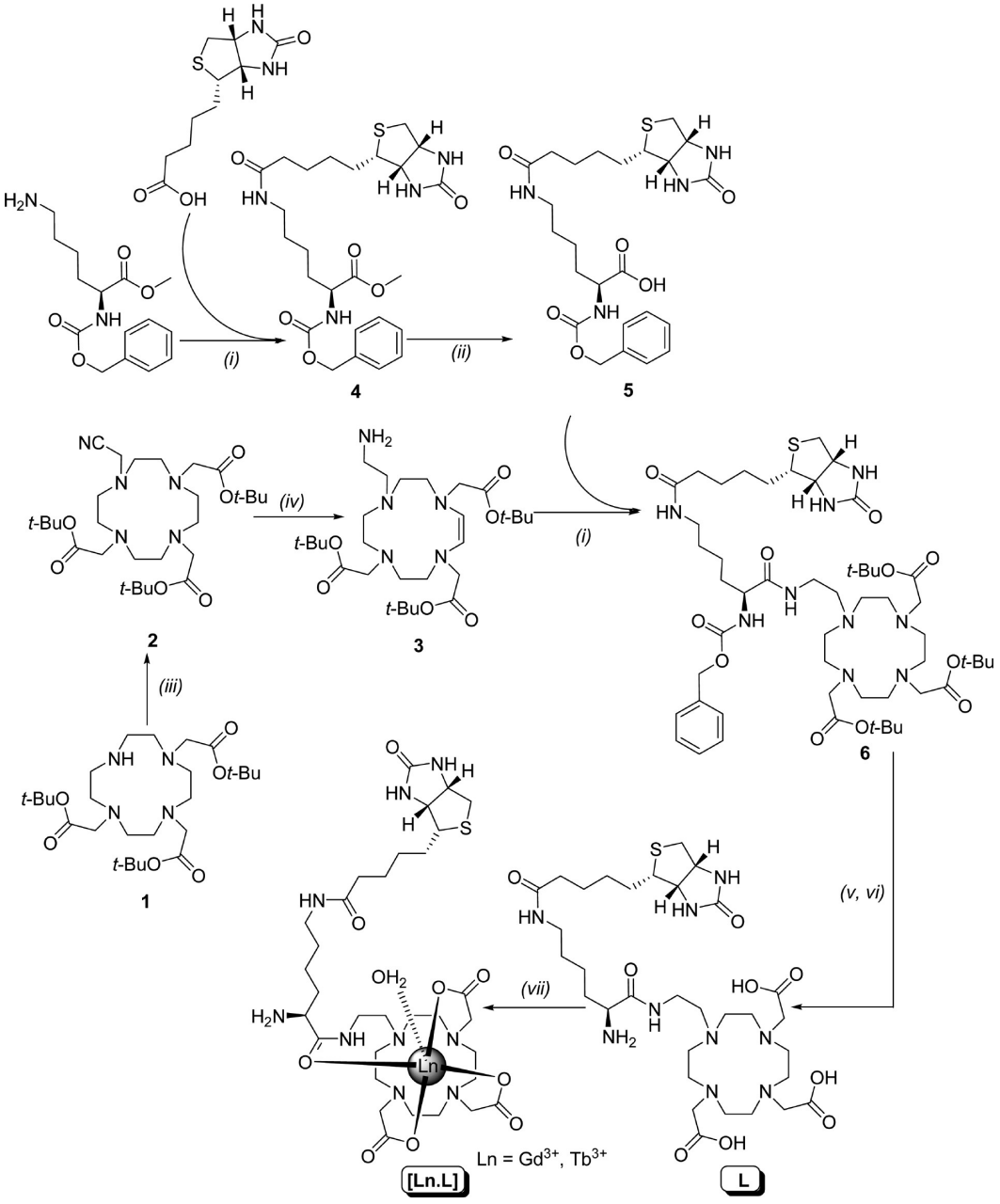

[a] Reagents and conditions: (i) NMM, EDC, HOBt, anhydrous DMF, 62% for **4** and 48% for **6**; (ii) LiOH, THF/MeOH/water (3:2:2) 67%; (iii) bromoacetonitrile, K_2CO_3, MeCN; (iv) Ra−Ni, H_2, 7 M NH_3/MeOH, 50 psi; (v) Pd−C (10%), H_2, MeOH, 50 psi; (vi) TFA (neat), 54%; (vii) $TbCl_3 \cdot 6H_2O$ or $GdCl_3 \cdot 6H_2O$, H_2O, pH 6.5, 80°C.

caged organic macrocyclic moiety [DO3A; (4,7-bis-carboxymethyl-1,4,7,10-tetraaza-cyclododec-1-yl)-acetic acid] as MR reporter, leaving the biotin moiety free for avidin binding and subsequent visualization with histological methods. This double functionality in a single molecule allows both in vivo longitudinal brain connectivity studies by means of MRI and postmortem microscopic investigation in the same experimental animal. Therefore, the macro- and microscopic aspects of a brain circuit can be simultaneously investigated. Compared to neuronal tracing with manganese,[8,9] the synthesized contrast agent is biocompatible and does not show signs of toxicity.

RESULTS AND DISCUSSION

Design and Synthesis of the Contrast Agent. The MR probe [**Gd.L**] contains GdDO3A-ethylamine (GdDO3A-EA) [22] and biocytin, where the primary amine of the macrocyclic moiety was coupled to the acid of biocytin via an amide bond. The synthesis of [**Gd.L**] was performed in seven steps prior to complexation with Gd^{3+} ions (Scheme 1). Stepwise alkylation of tris-*tert*-butyl-DO3A, **1**, with bromoacetonitrile in acetonitrile yielded nitrile **2**, which was reduced by hydrogenation using Ra−Ni as the catalyst in 7 M NH_3/MeOH in a Parr apparatus to

give **3**.[23] The intermediate **5** was synthesized by coupling the amine $^{\alpha}N$-carbobenzyloxy-L-lysine methyl ester and acid D-biotin [EDC/HOBt/NMM] in anhydrous DMF to obtain compound **4**, followed by selective deprotection of the methyl group with LiOH. The triester **6** was synthesized by coupling amine **3** and acid **5** [EDC/HOBt/NMM] in anhydrous DMF, from which **L** was obtained by successive deprotections (benzylcarbamate removal by hydrogenation using Pd−C as the catalyst and *tert*-butyl groups with neat TFA). Ligand, **L**, was purified by RP-HPLC and loaded with Gd^{3+} using $GdCl_3 \cdot 6H_2O$ and Tb^{3+} using $TbCl_3 \cdot 6H_2O$ in water at pH 6.5. The purity of final complex [**Gd.L**] was further analyzed by RP-HPLC, and the final concentrations of Ln^{3+} were determined by inductively coupled plasma optical emission spectrophotometry (ICP-OES).

Inner Sphere Hydration Number (*q*) Determination of [Tb.L]. The hydration state, *q*, of the analogous pair of the Tb complex was measured. This process involved determining the radiative lifetime of the Tb $^5D_4$ excited state in H_2O and D_2O. The empirical relationship was used that accounts for vibrational deactivation of the metal excited state by directly coordinated, closely diffusing water molecules and proximate NH oscillators.[24] Hence, *q* values were estimated. This data confirmed that the complex shows a *q* value ≤ 0.8, which clearly indicates the monoaqua Tb-coordinated system. It is known that this type of chelate is thermodynamically and kinetically stable.[15] Structurally related analogues (bearing N-linked CH_2CH_2NHCO- moieties) forming monoaqua ($q = 1$) species in solutions were previously reported.[23−25]

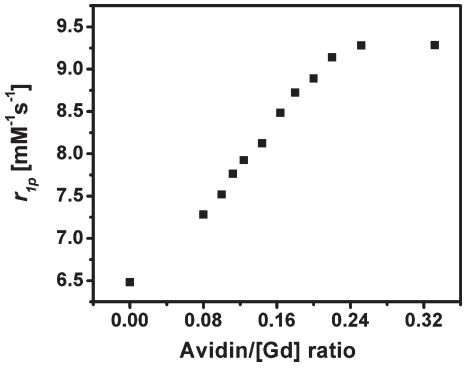

Figure 1. Variation of r_{1p} with added avidin for an aqueous solution containing [**Gd.L**] (21 °C, 128 MHz, pH 7.4, PBS, 0.25 mM complex).

Proton Relaxivity Modulation of [Gd.L] by Biotin−Avidin Interaction. We initially verified that the synthesized contrast agent retained the expected NMR properties and the avidin-binding affinity for histological detection was sufficient for the system to be considered as a potential bifunctional neuronal tracer. The proton longitudinal relaxivity (r_{1p}) of monoaqua complex [**Gd.L**] at 3T (128 MHz) [phosphate buffered saline (PBS), 7.4 pH, 21 °C] was 6.48 mM^{-1} s^{-1}, higher than the relaxivity reported for Gd-DO3A derivatives in such physiological solution in the literature.[26] The observed higher relaxivity in solution is explained by the high molecular volume and a significant second-sphere contribution due to the primary amine present in the molecule.[27,28]

To quantify the binding affinity of [**Gd.L**] to avidin, we performed MRI experiments at 3T (128 MHz) with incremental addition of avidin to constant concentrations of contrast agent (0.25 mM) and measured the r_{1p}. As expected, linear enhancement in r_{1p} (up to 43%; from 6.48 to 9.28 mM^{-1} s^{-1}) of [**Gd.L**] was observed upon binding to avidin (Figure 1). We obtained saturation in relaxivity at an approximate ratio of 4:1 for the [**Gd.L**]**:avidin** adduct, which confirms with the tetrameric nature of avidin.[29] This result is in agreement with the Solomon−Bloembergen−Morgan theory which predicts that at high magnetic fields the longitudinal relaxivity changes with the inverse of molecular rotational correlation time (τ_R) whereby an increase in relaxivity is expected upon binding of the contrast agent to a large molecule as avidin.[30] This trend was already reported in the literature for fast tumbling low molecular weight Gd^{3+}-chelates.[31,32] Thus, complex {[**Gd.L**]**:avidin**} (4:1) binding stoichiometry indicates that [**Gd.L**] could be easily visualized by tight binding with avidin via histological techniques.

Cellular Toxicity and Uptake Studies on N18 Murine Neuroblastoma Cells. We examined the biocompatibility of the synthesized contrast agent using cultured N18 differentiated murine neuroblastoma cells.[33] Differentiation was induced by serum deprivation and translated into a neuronal-like phenotype of the cell line including neuritic processes. First, [**Gd.L**] was tested for acute cytotoxicity under the same experimental conditions used in the following in vitro MRI experiments. Concentrations of [**Gd.L**] ranging from 10 to 50 μM in HBSS/10 mM HEPES were added to the cell cultures, and the state of the cells was tested 6 h later by visual inspection under microscopy and determination of cell numbers (using a fluorescent DNA stain and fluorescence spectroscopy). [**Gd.L**] did not induce any cytotoxic effects up to the highest dose (Figure 2A).

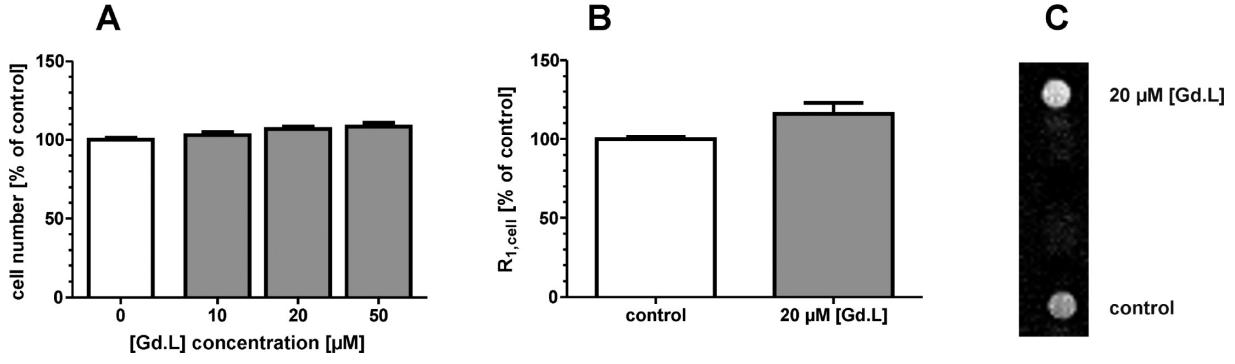

Figure 2. Toxicity and cellular uptake. Evaluation of the cytotoxicity of [**Gd.L**] in cultured murine N18 neuroblastoma cells (A). Enhancement of the cellular relaxation rate $R_{1,cell}$ by [**Gd.L**] (B), and representative T_1-weighted images of N18 cells labeled with [**Gd.L**] (C). Prior to incubation, N18 cells were morphologically differentiated by stepwise reduction of the FBS content to 1.25%. Cells were incubated with 10, 20, or 50 μM (A) or 20 μM (B, C) [**Gd.L**] in HBSS/10 mM HEPES for 6 h. Further processing of the sample was done as described in the Methods section.

In a second series of experiments the effect of [**Gd.L**] on the viability of differentiated N18 cells was determined. For this purpose, the metabolic activity (activity of intracellular dehydrogenases) was determined after a 24 h treatment with 5−150 μM [**Gd.L**]. Only at concentrations ≥ 100 μM a statistically significant reduction of metabolic activity and thus viability of N18 cells could be observed (Supporting Information, Figure S1A). However, even at 150 μM, metabolic activity was only reduced about 20%. Under certain circumstances, metabolic activity can change independently of the number of cells. Thus, the number of cells was additionally determined in the same experimental setup. Similar results were obtained (Supporting Information, Figure S1B) indicating that for [**Gd.L**] metabolic activity/viability and cell number were correlated. All further in vitro experiments were performed at concentrations below 50 μM.

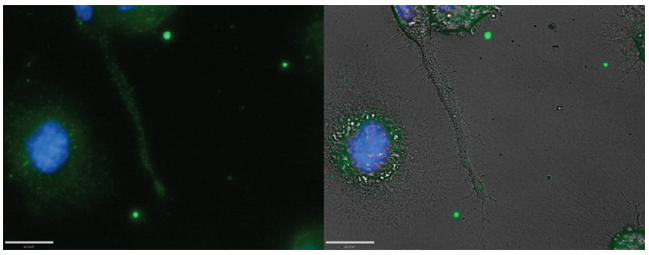

Figure 3. Optical evidence for intracellular localization of [**Fluo.L**] in N18 neuroblastoma cells. Cells were incubated with 25 μM [**Fluo.L**] for 12 h in culture medium (DMEM, 0.625% FBS) as described in the Methods section. Overlay of green (FITC in [**Fluo.L**]) and blue fluorescence (DNA dye Hoechst 33342) (left) and in addition to the phase contrast image (right). The bar represents 20 μm.

We next investigated whether the cellular permeability of biocytin is retained in the synthesized contrast agent. Differentiated N18 cells were incubated with [**Gd.L**] at 20 μM for 6 h. After incubation, the extensively washed cells were trypsinized and transferred to Eppendorf tubes at a density of 1×10^7 cells/500 μL. Cellular relaxation rate $R_{1,cell}$ was determined in an axial slice of the cell pellet at 3T (128 MHz). A significant increase in the relaxation rate ($R_{1,cell}$ = 116% of control) of the cells was observed (Figure 2B) indicating cellular internalization of the contrast agent. Contrast agent uptake was also apparent in the signal intensity of corresponding T_1-weighted images of the cell pellets (Figure 2C).

The intracellular localization of [**Gd.L**] cannot be directly assessed by MRI. To further prove that the contrast agent was internalized and distributed inside the cells and not only binding to the cell surface, a fluorophore containing analogue [**Fluo.L**] was used. Differentiated N18 cells were incubated with [**Fluo.L**] for 12 h, and remaining extracellular fluorescence was quenched by Trypan Blue,[34] followed by extensive washing. Fluorescence microscopy displayed that [**Fluo.L**] was internalized very quickly and mainly accumulated in vesicles in the perinuclear region of the cells (Figure 3). Green fluorescence of [**Fluo.L**] could also be detected in the projections of the cells. These results indicate a distinct and predominantly endosomal uptake of [**Fluo.L**] into morphologically differentiated neuroblastoma cells as well as transport along the projections to their terminals.

In Vivo Uptake and Transport: MR and Histology Studies of [Gd.L] in Rat Brain. We finally investigated the tracing ability of the newly synthesized imaging probe [**Gd.L**] by means of MRI and classical histological methods. We performed a series of pressure injections into the primary motor cortex (M1) of anesthetized albino rats (Sprague−Dawley) and evaluated the

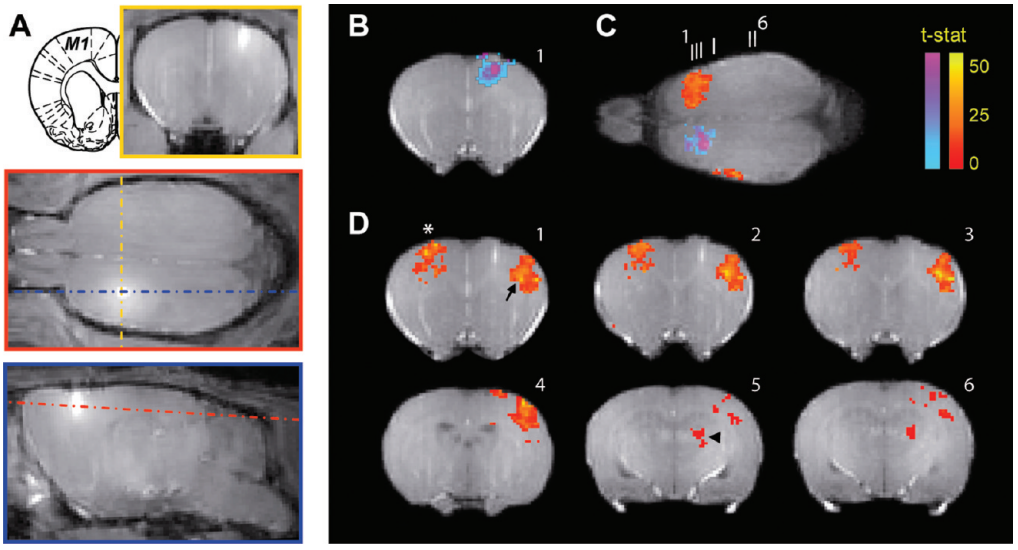

Figure 4. In vivo neuronal tract tracing with [**Gd.L**]. Neuronal connections of the primary motor cortex M1 of the rat were investigated in individual animals. (A) Coronal (yellow line), horizontal (red line), and sagittal (blue line) T_1-weighted images acquired 30 min after the injection of [**Gd.L**] in M1. Note the enhanced signal (bright spot) at the injection site. The inset shows a representative scheme of rat brain anatomy at the coordinates of the injection (Paxinos and Watson, 2007).[35] (B−D) Shown are coronal (B, D) and horizontal (C) MR images illustrating the distribution of [**Gd.L**] signal in the brain of a representative animal (same as in A) after an injection in M1. The presence of signal is shown as statistical maps (unpaired *t* test; $p < 0.01$) comparing the baseline (preinjection scans) and scans acquired 30 min (blue-purple maps) or 24 h (orange-yellow maps) later, superimposed on the anatomical images. Five images were acquired at each time point (see Methods). The results demonstrate local increases in signal due to [**Gd.L**] injection (B, C) and long-range neuronal tract-tracing after 24 h (C, D). White numbered bars in (C) indicate the position of coronal images in (B) and (D). The white asterisk, black arrow, and arrowhead indicate the retrograde neuronal connections from M1 to the contralateral M1, ipsilateral cortex, and thalamus, respectively. After the last MRI session, the animal was euthanized and the histology is shown in Figure 5. Paxinos, G., Watson, C., 2007. The rat brain in stereotaxic coordinates, 6 ed. Academic Press, Elsevier as ref 36.

transport of the probe at 24 and 48 h postinjection (for details on the injections, see the Methods section).

Figure 4 shows the results of a representative experiment in one animal in which [**Gd.L**] was injected into the M1 cortex. Immediately after administration, the injection site is clearly visualized in T_1-weighted MR images and the coordinates of the stereotaxic injection verified (Figure 4A). Statistical analysis comparing baseline images (acquired either before or immediately after the injection) with images acquired after 24 and 48 h revealed significant increase in T_1-weighted signal intensity in different brain regions. These regions are known to be connected with M1, such as the thalamus, the homologous contralateral M1 cortex, and other ipsilateral cortical regions (Figure 4B−D). Similar results were obtained in all injected animals (n = 4). These observations clearly corroborate the neuronal-tracing ability of [**Gd.L**] and its suitability for in vivo studies of brain connectivity. Post-mortem histological investigations in the same animals verified the neuroanatomical projections found in vivo with MRI (Figure 5).

As expected, the histological results also added important information about the cells forming the projections and with a spatial resolution that cannot be obtained by applying only MRI. For instance, the morphology and precise position in the cortical column of the cells projecting to the injection site (retrogradely stained with the tracer) (Figure 5E), the axonal trajectories of the connected neurons (Figure 5D), or their thalamic localization in the ventrolateral nucleus (Figure 5G) could be revealed in the same experimental subjects. These anatomical details would be difficult to obtain from MR images alone. The fact that the morphology of the retrogradely stained neurons (Figure 5E and F) is well retained provided further evidence for the absence of toxic effects, therefore supporting its applicability in longitudinal experiments in which brain networks are repeatedly investigated, for instance, in monitoring the progression of a brain disease in an animal model.

Biocytin is a well-known anterograde as well as retrograde neuronal tract tracer after extracellular injection in the brain.[7] However, not much is known about the uptake and transport mechanisms of biocytin at high concentrations. Baur et al. reported a specific, fast, and sodium-dependent high affinity uptake for a neuroblastoma cell line which could not be found in glioma cells.[36] Its saturation kinetic was in a low concentration range. However, under physiological conditions, the biocytin concentration in the brain is well below the reported concentration at half maximal saturation (K_m) of the biocytin uptake.[36] On the contrary, after pressure or iontophoretic injection, local concentrations exceed the physiological concentration of biocytin manifold. Thus, the uptake mechanism under such conditions is not established. In addition, it must be mentioned that, in contrast to biocytin, the experiments performed with [**Gd.L**] only demonstrated retrograde transport, with the exception (only seen under the microscope in histological preparations) of axons going down to the brain stem via the striatum bundles and internal capsule (Figure 5F), but without showing any terminal ramifications. It is conceivable that the modifications introduced in the model molecule biocytin described above, together with the significant increase in molecular weight by about the factor 2.5, substantially alter the uptake and transport properties of the resulting contrast agent. Under physiological pH conditions, it is expected that [**Gd.L**] is positively charged due to primary amine, which can have a significant influence on the interaction with cellular membranes. The cellular uptake and distribution experiments performed with

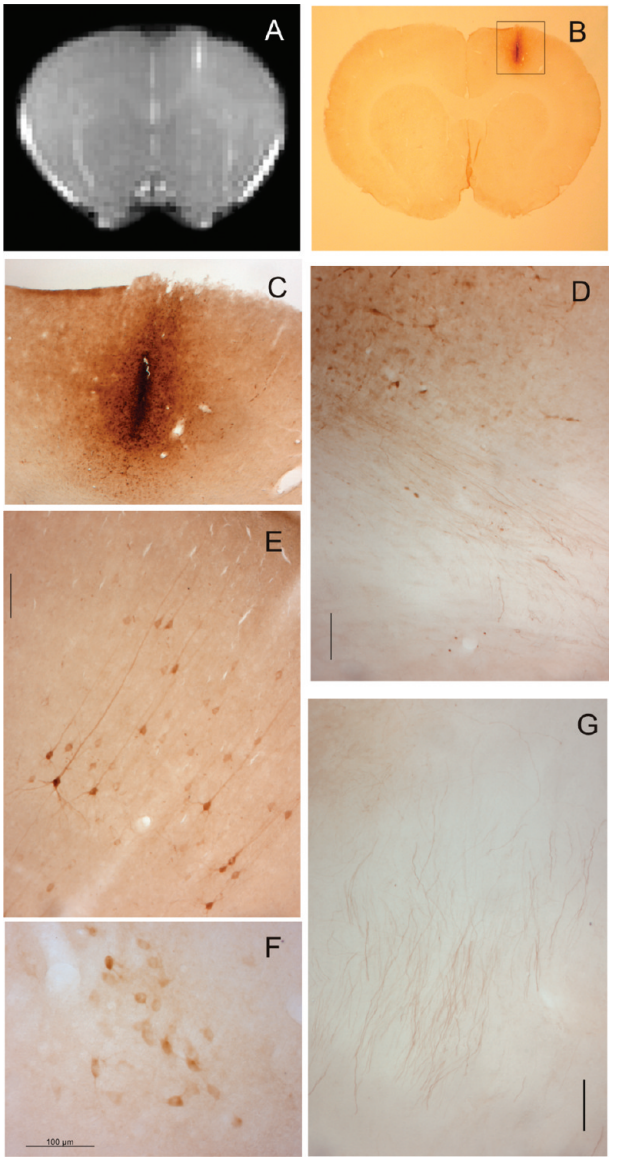

Figure 5. Histology of the brain shown in Figure 4 after 48 h. (A) Same as in Figure 4A, showing the injection site with MRI (white spot in the cortex). (B, C) Injection site under the microscope after histological treatment with avidin and visualization with diaminobenzidine. (D) Axonal transport in the white matter beneath the injection site. (E) Retrogradely stained neurons in the cortex lateral from the injections site, corresponding to the location indicated by the black arrow in Figure 4D. (F) Retrogradely stained neurons in the thalamus, corresponding to the location indicated by the arrowhead in Figure 4D. (G) Anterogradely stained axons in the internal capsule (not visible in MRI). Bars: 0.1 mm.

the fluorescent analogue of [**Gd.L**] point to a primarily endocytotic internalization of the probe into differentiated N18 neuroblastoma cells (Figure 3). This change in internalization mechanism and the consequently dissimilar intracellular distribution of [**Gd.L**] might explain the predominantly retrograde transport compared to biocytin.

In summary, we have obtained the first neuronal tracer with paramagnetic properties that preferentially stains retrograde connections, further extending the possibilities of MRI tract-tracing in vivo.

SIGNIFICANCE

The results we report here represent a new platform for the development of multimodal molecular imaging tools of broad interest in neuroscience. We have presented the synthesis and characterization of a new generation of Gd-containing biocytin-based imaging probes that capture in vivo the dynamics of large scale neural networks together with their cellular characteristics and microcircuitry, thereby spanning several organizational levels. We present data that demonstrate the validity of the approach by showing brain networks of cortical connectivity in vivo applying T_1-weighted MRI together with the corresponding cellular details, such as fibers and neuronal morphology, under light microscopy. Comparing MRI with histological tracings, we demonstrate that the synthesized imaging probe preferentially stains retrograde projections, thus extending the possibilities of MRI tract-tracing in vivo with the first retrograde tracer.

METHODS

Chemicals. All solvents and reagents were purchased at analytical grade from commercial suppliers (Acros, Aldrich, Fluka, Merck, Strem and VWR) and were used without further purification unless otherwise stated. 2,3-Bis(2-methoxy-4-nitro-5-sulfophenyl)-2*H*-tetrazolium-5-carboxanilide inner salt (XTT) and *N*-methylphenazonium methyl sulfate (PMS) were procured from Sigma Aldrich (Germany). All air- or water-sensitive chemicals were stored under an inert atmosphere. Ultrapure deionized water (18 MΩ cm^{-1}) was used throughout.

Chromatography. Flash column chromatography was performed using silica gel 60 (70−230 mesh) from Merck. Thin layer chromatography (TLC) was performed on aluminum sheet silica gel plates with 0.2 mm thick silica gel 60 F_{254} (E. Merck) using different mobile phases. The compounds were visualized by UV irradiation (254 nm) or iodine staining.

Reverse phase high performance liquid chromatography (RP-HPLC) was performed at room temperature on Varian PrepStar and Perkin-Elmer Instruments. UV absorbance was measured at 214 nm. Semipreparative RP-HPLC was performed on a stainless steel Chromsep (length 250 mm, internal diameter 21.2 mm, and particle size 5 μm) C_{18} column (Varian). The compound was purified using Method A: gradient with the mobile phase starting from 95% solvent A (H_2O) and 5% solvent B (MeOH) to 70% B in 10 min, 90% B in 18 min, 90% B isochratic until 22 min and decreased to 5% B in 26 min. To check the purity of the final complex, analytical HPLC was carried out on a 150 × 4.66 mm 4micron Phenomenex Synergi 4u Fusion-RP 80i column using Method B: 95% solvent A (H_2O, 0.1% HCOOH) and 5% solvent B (MeCN, 0.1% HCOOH) isochratic for 2 min, 5% B to 100% solvent B in 15 min and then running isocratic for 2 min and then back to 5% solvent B in the next 5 min. The flow rate generally used for analytical HPLC was 1 mL/min and for semipreparative HPLC 15 mL/min. All the HPLC-grade solvents for HPLC were filtered through a nylon-66 Millipore filter (0.45 μm) prior to use.

Spectroscopy. ^{1}H NMR and ^{13}C NMR spectra were recorded on Bruker DRX250 and DRX400 spectrometers at room temperature. The ^{1}H NMR chemical shifts were adjusted to the residual protons of the solvent peaks which were referenced to TMS (0.0 ppm), and ^{13}C NMR chemical shifts were referenced to $CDCl_3$ (77.0 ppm).

Electrospray mass spectra (ESI-MS in positive and negative ion mode) were acquired on an ion trap SL 1100 system (Agilent, Germany), and high resolution (HR) mass spectra were measured on a Bruker Daltonics Apex II FT-ICR-MS instrument (Bruker, Germany).

Inductively coupled plasma optical emission spectrometry (ICP-OES) for the evaluation of the Gd^{3+} concentration was performed using a Jobin−Yvon Ultima 2 spectrometer.

Lifetime was measured on a Perkin-Elmer LS55 luminescence spectrometer (using FL Winlab software). Sample was contained in quartz cuvettes with a path length of 1 cm and polished base.

Inner Sphere Hydration Number (*q*) Determination. Inner sphere hydration numbers (q) were determined after excitation at the $^5D_4 \leftarrow {}^7F_6$ band (488 nm) and emission at 545 nm. A 5 mM solution of Tb-complex was prepared at pH 7.4 in H_2O and in D_2O. Hydration number, q, was calculated according to the eq 1.

$$q_{Tb} = 5\left[(k_{H_2O} - k_{D_2O} - 0.06) - 0.01n\right] \quad (1)$$

In the case of coordinated amide NH oscillators present close to the lanthanide ion, another correction is made in order to obtain q (eq 1), where n refers to the number of amide NH oscillators.

In Vitro MR Tube Measurements. Four different concentrations (1, 0.75, 0.5, 0.25 mM) of [**Gd.L**] were prepared in phosphate buffered saline (PBS-Dulbecco's) in 1.5 mL Eppendorf tubes at physiological pH to measure relaxivity. Each tube was filled with 400 μL of the CA solution.

MR tube measurements were performed on a clinical 3T (128 MHz, 21 °C) human MR scanner (MAGNETOM Tim Trio, Siemens Healthcare, Germany). Longitudinal relaxation times (T_1) were measured using an inversion recovery sequence to obtain images from a 2 mm thick slice through the samples. The inversion time was varied from 23 to 3000 ms in about 12 steps. The images were read out with a turbo spin echo technique, acquiring 5 echoes per scan. The repetition time TR was 10 s to ensure complete relaxation between the scans. A resolution of 256 × 256 voxels over a field-of-view of 110 × 110 mm^2 was reached. Six averages were acquired within less than 25 min.

To measure the changes in longitudinal relaxivity (r_1), MRI experiments were performed with increasing concentrations of avidin proportional to a constant concentration of [**Gd.L**] (0.25 mM) incubated for 1 h at 37 °C. The stock solution of avidin (1 mM) was prepared in PBS at pH 7.4.

Axial images were obtained for the set of tubes at the respective magnetic fields, and the T_1 values were then calculated.

Relaxivity at different concentration of avidin was then calculated using eq 2.

$$r_{1,obs} = (1/T_{1,obs} - 1/T_{1,d})/[\mathbf{Gd.L}] \quad (2)$$

where $T_{1,obs}$ is the measured T_1, $T_{1,d}$ is the diamagnetic contribution of the solvent (calculated to be 2500 ms), and [**Gd.L**] is the concentration in mmol of the appropriate Gd(III) complex.

Synthesis of ligand. *(S)-Methyl 2-(Benzyloxycarbonylamino)-6-(5-((3aS,4S,6aR)-2-oxo-hexahydro-1H-thieno[3,4-d]imidazol-4-yl)-pentanamido)hexanoate (**4**).* A solution of $^{\alpha}$*N*-carbobenzyloxy-L-lysine methyl ester (2 g, 6.8 mmol), biotin (1.7 g, 6.9 mmol), NMM (1.5 mL, 14.9 mmol), and HOBt (1.44 g, 7.5 mmol) in DMF (5 mL) was stirred at 0−5 °C for 15 min. EDC (1.01 g, 7.5 mmol) was added. The reaction mixture was stirred overnight at room temperature. Completion of the reaction was verified by ESI-MS, and the solution was poured into water (100 mL) and extracted with EtOAc (3 × 100 mL). The combined organic layers were dried over anhydrous Na_2SO_4 and filtered, and the filtrate was evaporated under reduced pressure. The residue was purified by column chromatography (silica gel, 8% MeOH in CH_2Cl_2, R_f = 0.45) to give **4** as transparent sticky solid (2.19 g, 62%). ^{1}H NMR ($CDCl_3$, 400 MHz), δ (ppm): 1.25−1.36 (m, 4H); 1.37−1.47 (m, 2H); 1.50−1.67 (m, 5H); 1.68−1.79 (m, 1H); 2.09 (t, J = 7.5 Hz, 2H); 2.54−2.62 (m, 1H); 2.70−2.80 (m, 1H); 2.97−3.04 (m, 1H); 3.05−3.18 (m, 2H); 3.65 (s, 3H); 4.11−4.18 (m, 1H); 4.19−4.27 (m, 1H); 4.31−4.37 (m, 1H); 5.02 (s, 2H); 5.98 (s, 2H); 6.56 (t, J = 7.0 Hz, 1H); 6.73 (s, 1H); 7.19−7.32 (m, 5H). ^{13}C NMR ($CDCl_3$, 100 MHz), δ (ppm): 22.5; 25.6; 27.9; 28.2; 28.8; 31.7; 35.8; 38.7; 40.4; 52.3; 53.7; 55.7; 60.1; 61.7; 66.8; 127.9; 128.1; 128.4; 136.2; 156.2; 164.3;

173.2; 173.4. ESI-HRMS (+): calcd $C_{25}H_{36}N_4O_6S$, m/z 521.2428 $(M + H)^+$; found, 521.2429 $(M + H)^+$.

*(S)-2-(Benzyloxycarbonylamino)-6-(5-((3aS,4S,6aR)-2-oxo-hexahydro-1H-thieno[3,4-d]imidazol-4-yl)pentanamido)hexanoic acid (**5**).* A solution of (*S*)-methyl 2-(benzyloxycarbonylamino)-6-(5-((3a*S*,4*S*,6a*R*)-2-oxo-hexahydro-1*H*-thieno[3,4-*d*]imidazol-4-yl)pentanamido)hexanoate (2 g, 3.8 mmol) in 50 mL of THF/MeOH/water (3:2:2) was stirred at 0−5 °C for 15 min, and then LiOH (0.18 g, 7.7 mmol) was added. The reaction mixture was stirred for 2 h at room temperature. Completion of the reaction was verified by ESI-MS, and the reaction mixture was concentrated under reduced pressure. The compound was purified by preparative RP-HPLC (Method A, λ = 214 nm, t_R = 14 min). After lyophilization, **5** was obtained as white powder (1.3 g, 67%). ^{1}H NMR ($CDCl_3$, 250 MHz), δ (ppm): 1.22−1.34 (m, 4H); 1.35−1.45 (m, 2H); 1.50−1.67 (m, 5H); 1.66−1.75 (m, 1H); 2.01 (t, J = 7.5 Hz, 2H); 2.50−2.60 (m, 1H); 2.68−2.78 (m, 2H); 2.94−3.00 (m, 1H); 3.01−3.12 (m, 2H); 4.06−4.12 (m, 1H); 4.14−4.22 (m, 1H); 429−4.35 (m, 1H); 5.09 (s, 2H); 5.82 (s, 2H); 6.42−6.47 (m, 1H); 6.69 (s, 1H); 7.16−7.32 (m, 5H). ^{13}C NMR ($CDCl_3$, 62.9 MHz), δ (ppm): 22.5; 25.6; 27.9; 28.2; 28.8; 31.7; 35.8; 38.7; 40.4; 52.3; 53.7; 55.7; 60.1; 61.7; 66.8; 127.9; 128.1; 128.4; 136.2; 156.2; 164.3; 173.2; 173.4. ESI-HRMS (+): calcd $C_{24}H_{34}N_4O_6S$, m/z 507.2278 $(M + H)^+$; found, 507.2279 $(M + H)^+$.

*[4,7-Bis-butoxycarbonylmethyl-10-(2-((S)-2-(benzyloxycarbonylamino)-6-(5-((3aS,4S,6aR)-2-oxo-hexahydro-1H-thieno[3,4-d]imidazol-4-yl)-pentanamido)hexanamido)ethyl)-1,4,7,10-tetraaza-cyclododec-1-yl] Acetic Acid tert-Butyl Ester (**6**).* A solution of [4,7-bis-butoxycarbonylmethyl-10-(2-aminoethyl)-1,4,7,10-tetraazacyclododec-1-yl] acetic acid *tert*-butyl ester (0.88 g, 1.58 mmol), (*S*)-2-(benzyloxycarbonylamino)-6-(5-((3a*S*,4*S*,6a*R*)-2-oxo-hexahydro-1*H*-thieno[3,4-*d*]imidazol-4-yl)pentanamido) hexanoic acid (0.8 g, 1.58 mmol), NMM (0.35 mL, 3.4 mmol), and HOBt (0.33 g, 1.74 mmol) in anhydrous DMF (5 mL) was stirred at 0−5 °C for 15 min, and then EDC (0.23 g, 1.74 mmol) was added. The reaction mixture was stirred overnight at room temperature. Completion of the reaction was verified by ESI-MS, after which the solution was poured into water (50 mL) and extracted with EtOAc (3 × 50 mL). The combined organic layers were dried over anhydrous Na_2SO_4 and filtered, and the filtrate was evaporated under reduced pressure. The residue was purified by column chromatography (silica gel, 10% MeOH in CH_2Cl_2, R_f = 0.15) to give **6** as a dark yellow sticky solid (0.76 g, 48%). ^{1}H NMR ($CDCl_3$, 250 MHz), δ (ppm): 1.13−1.27 (m, 4H); 1.22 (s, 18H); 1.42 (s, 9H); 1.51−1.89 (m, 8H); 1.98 (t, J = 7.5 Hz, 2H); 2.10−2.38 (m, 1H); 2.42−3.18 (m, 19H); 3.22−3.37 (m, 2H); 3.39−3.44 (m, 1H); 3.48−3.97 (m, 8H); 4.02−4.10 (m, 1H); 4.11−4.20 (m, 1H); 427−4.31 (m, 1H); 5.04 (s, 2H); 5.27 (s, 2H); 5.57−5.67 (m, 1H); 6.30−6.52 (m, 2H); 7.20−7.50 (m, 5H). ^{13}C NMR ($CDCl_3$, 62.9 MHz), δ (ppm): 17.9; 18.5; 22.7; 23.3; 28.2; 29.4; 29.7; 31.9; 33.4; 39.8; 41.1; 48.4; 50.2; 51.8; 52.3; 53.6; 56.2; 56.6; 56.7; 56.9; 60.1; 62.0; 66.6; 81.9; 82.1; 127.8; 128.1; 128.5, 135.6; 155.6; 161.9; 169.7; 169.9; 170.4; 173.7. ESI-HRMS (+): calcd $C_{52}H_{87}N_9O_{11}S$, m/z 1046.6318 $(M + H)^+$; found, 1046.6320 $(M + H)^+$.

*[4,7-Bis-carboxymethyl-10-(2-((S)-2-amino-6-(5-((3aS,4S,6aR)-2-oxo-hexahydro-1H-thieno[3,4-d]imidazol-4-yl)pentanamido)hexanamido)-ethyl)-1,4,7,10-tetraaza-cyclododec-1-yl] Acetic Acid (**L**).* A solution of [4,7-bis-butoxycarbonylmethyl-10-(2-((*S*)-2-(benzyloxycarbonylamino)-6-(5-((3a*S*,4*S*,6a*R*)-2-oxo-hexahydro-1*H*-thieno[3,4-d]imidazol-4-yl)-pentanamido)hexanamido)ethyl)-1,4,7,10-tetraazacyclododec-1-yl] acetic acid *tert*-butyl ester (0.7 g, 0.67 mmol) and 10% Pd−C (0.18 g) under H_2 (50 psi) in MeOH (20 mL) was stirred at room temperature in a Parr apparatus for 8 h. Completion of the reaction was verified by ESI-MS, the solvent was filtered through a G-4 sintered funnel, and the filtrate was evaporated under reduced pressure. This crude product was further dissolved in CH_2Cl_2/TFA (8 mL + 2 mL) and stirred at room temperature for 20 h. Completion of the reaction was verified by ESI-MS; the solvent was evaporated under reduced pressure and dissolved in a minimum volume of MeOH (1 mL) followed by dropwise addition of diethylether at 0−5 °C and stirring for 30 min at room temperature. The compound was precipitated and filtered through a G-4 sintered funnel under nitrogen. The precipitate was dissolved in water and neutralized by adding 1 M NaOH. The crude product was then purified by preparative RP-HPLC (t_R = 2.9 min) to get **L** as a yellow sticky solid (0.26 g, 54%). ^{1}H NMR (D_2O, 250 MHz), δ (ppm): 1.31−2.08 (m, 12H); 2.24 (t, J = 7.0 Hz, 2H); 2.60−4.30 (br. m, 31H); 4.33−4.48 (m, 1H); 4.50−4.53 (m, 1H); 4.54−4.58 (m, 1H). ^{13}C NMR (D_2O, 62.9 MHz), δ (ppm): 19.4; 20.4; 22.9; 25.4; 25.6; 27.9; 33.3; 33.8; 34.2; 34.5; 36.5; 37.4; 45.4; 46.7; 48.9; 50.9; 53.0; 54.2; 56.5; 58.0; 59.8; 162.7; 172.8; 173.1; 173.5; 179.4. ESI-MS (+): calcd $C_{32}H_{57}N_9O_9S$, m/z 744.4 $(M + H)^+$; found, 744.5 $(M + H)^+$.

*General Preparation of Lanthanide Complexes of **L**.* Lanthanide complexes of **L** were prepared from corresponding solutions of the ligand (1 equiv) and solution of $GdCl_3.6H_2O$/$TbCl_3 \cdot 6H_2O$ (1.1 equiv). The reaction mixtures were stirred at 60 °C for 20 h. The pH was periodically checked and adjusted to 6.5 using solutions of NaOH (0.1 M) and HCl (0.1 M) as needed. After completion, the reaction mixtures were cooled and passed through chelex-100 to trap free Ln^{3+} ions, and the Ln-loaded complexes were eluted. The fractions were dialyzed (500 MW cutoff; Spectra/Pro biotech cellulose ester dialysis membrane, Spectrum Laboratories) and lyophilized to obtain a light yellowish solid. The absence of free Ln^{3+} was checked with xylenol orange indicator. The complexes were characterized by ESI-MS in positive mode, and the appropriate isotope pattern distributions for Ln^{3+} were recorded. The purity of the final complex was then analyzed by analytical RP-HPLC (t_R = 9.5 min).

[**Gd.L**] ESI-MS (+): calcd $C_{32}H_{54}{}^{155}GdN_9O_9S$, m/z 896.3 $[M + H]^+$; found, 896.3 $[M + H]^+$; r_{1p} = 6.48 $[mM^{-1}s^{-1}]$ at 128 MHz (1.4T). [**Tb.L**] ESI-MS (+): calcd $C_{32}H_{54}{}^{159}TbN_9O_9S$, m/z 900.3 $[M + H]^+$; found, 900.2 $[M + H]^+$; $\tau_{(H_2O)}$ 1.90 ms, $\tau_{(D_2O)}$ 3.40 ms, and q = 0.8.

In Vitro Cell Studies of [Gd.L]. *Cell Culture.* N18 mouse neuroblastoma cells were cultured as a monolayer at 37 °C with 5% CO_2 in antibiotic-free Dulbecco's modified Eagle's medium (DMEM) supplemented with 10% fetal bovine serum (FBS) and 4 mM L-glutamine (all purchased from Biochrom AG, Germany). Cells were passaged by trypsinization with trypsin/EDTA 0.05/0.02% (w/v) in PBS for 5 min every second to third day. In order to induce a neuronal phenotype, the FBS content was reduced stepwise to 1.25%[33] prior to the experiments. As a consequence, the growth rate slowed down and cells showed a flat morphology with a network of neurite-like processes which were completely absent at 10% FBS (data not shown).

*Cytotoxicity of [**Gd.L**].* Differentiated N18 cells were inoculated into 96-well plates and treated 48 h later with 10, 20, or 50 μM of the CA in HBSS/10 mM HEPES for an additional 6 h. Afterward, the cells were incubated with Bisbenzimid 33342 (Hoechst 33342), a nuclear stain, in order to assess the DNA content per well (correlating with the number of cells).[37,38] Cells were washed with HBSS, and the cell number-related fluorescence (Ex 346 nm/Em 460 nm) of the DNA dye was measured in a multiplate reader.

For the evaluation of long-term viability, differentiated N18 cells were incubated in 96-well plates and treated 24 h later with 5−150 μM of the CA in complete cell culture medium (DMEM containing 1.25% FBS). Afterward, metabolic activity as a marker for cell viability was determined by XTT-based colorimetric assay. Briefly, medium was removed and cells were further incubated for 30 min in DMEM (without phenol red and [**Gd.L**]) containing XTT (0.25 mM) and PMS (0.5 μM). Cells were thoroughly shaken to dissolve the formed water-soluble formazan dye, and the absorbance of the solution was measured at 450 nm and with reference wavelength at 690 nm in a multiplate reader. In order to test if the metabolic activity is correlated with the number of cells the formazan containing supernatant was then discarded and cells were incubated with Hoechst 33342 as described above.

*MRI on [**Gd.L**]-Labeled Cells.* For MRI, serum deprived N18 cells were grown in 175 mL tissue culture flasks for 3−4 days in complete culture medium. Afterward, cells were labeled with 20 μM [**Gd.L**] in HBSS/10 mM HEPES for an additional 6 h. Cells similarly incubated in the absence of [**Gd.L**] served as control. Cells were washed twice with HBSS and once with PBS (without Ca^{2+} and Mg^{2+}) followed by trypsinization. Subsequently, cells were counted (cell viability was assessed by trypan blue staining), centrifuged, and resuspended in complete culture medium at a cell density of 1×10^7 cells/500 μL and transferred to 0.625 mL Eppendorf tubes. Before performing MR measurements, cells were allowed to settle in the tubes. Cell pellets were imaged at room temperature (~21 °C) with a clinical 3T (128 MHz) human MR scanner (MAGNETOM Tim Trio, Siemens Healthcare, Germany), using a 12-channel RF head coil and slice selective measurements from a slice with a thickness of 1 mm positioned through the cell pellet. Relaxation times (T_1) were measured using an inversion−recovery sequence, with an adiabatic inversion pulse followed by a turbo-spin−echo readout. Numbers of MR images acquired were in the range 10−15, with the time between inversion and readout varying from 23 to 3000 ms. With a repetition time of 10 s, 15 echoes were acquired per scan and averaged six times. All experiments scanned 256^2 voxels in a field-of-view of 110 mm in both directions, resulting in a voxel volume of $0.6 \times 0.6 \times 1$ mm^3.

Data analysis was performed by fitting of relaxation curves with self-written routines under MATLAB 7.1 R14 (The Mathworks Inc.). The series of T_1 relaxation data were fitted to the following equation:

$$T_1 \text{ series with varying } t = T_1 : S = S_0\left(1 - \exp(-t/T_1)\right) + S_{(T_1=0)} \exp(-t/T_1)$$

Nonlinear least-squares fitting of three parameters S_0, $S_{(T_1=0)}$, and T_1 was done for manually selected regions of interest with the Trust-Region Reflective Newton algorithm implemented in MATLAB. The quality of the fit was controlled by visual inspection and by calculating the mean errors and residuals. The obtained T_1 values of the cell pellet were converted to $R_{1,\text{cell}}$ ($= 1/T_1$). These were expressed as percent of control ($R_{1,\text{cell}}$ of cells incubated under similar conditions in the absence of CA).

Live Cell Imaging. Fluorescence microscopy was done as described recently.[39] Briefly, already differentiated N18 cells (3×10^5 cells/mL) were inoculated and cultured in single channel Ibidi slides (Ibidi GmbH, Germany) until reaching 70−80% confluency using DMEM supplemented with 0.625% fetal bovine serum and 4 mM L-glutamine (all purchased from Biochrom AG, Germany). Cells were incubated with 25 μM [**Fluo.L**] for 12 h and counterstained with the nuclear dye Bisbenzimid 33342 (Hoechst 33342), and extracellular fluorescence was quenched by the addition of ice-cold Trypan Blue.[34] After repeated cell washings with Hanks' buffered saline (HBSS, Biochrom AG, Germany), fluorescence microscopy was performed on a Zeiss Axiovert 200 M instrument (Carl Zeiss AG, Germany) with a Plan-Apochromat 63× objective to observe the cellular localization and distribution of [**Fluo.L**] by irradiating with blue light (470 nm) and observing at 525 nm. Nuclear labeling by Hoechst was observed at 460 nm. Phase contrast images with differential image contrast (DIC) of the same area were made to observe if the cells maintain their normal morphology in the presence of [**Fluo.L**].

In Vivo Rat Experiments. We performed pressure injections of probe [**Gd.L**] into the primary motor cortex of four albino rats (Sprague−Dawley). Three of them with [**Gd.L**] were sacrificed after 24 h and the remaining one with [**Gd.L**] after 48 h. All surgical and experimental procedures were approved by the local authorities (Regierungspraesidium, Tuebingen) and are in full compliance with the directive of the European community for the protection of animals used for experimental and other scientific purposes (86/609/EEC).

Injections. All rats were anaesthetized with 2% isoflurane (Abbott, Germany) and placed in a stereotaxic frame (Kopf Instruments). After additional use of xylocain for local analgesia in the surgery area, a craniotomy was performed and a pulled fused silica capillary (ID 50 μm; OD 150 μm; tip diameter 20−30 μm) was placed in the primary motor cortex at a depth of 1.2 mm below the surface. Complex was then injected per animal using a pressure cell containing the compound attached to the other end of the fused silica capillary. An amount of 100 nL of 4% tracer solution (containing 4.5 nmol tracer) was injected at a flow rate of 3.33 nL/min (about 0.15 nmol/min). After injection, the capillary was left in place for 10 min before retracting it stepwise to avoid backflow of the injected solution.

At the end of the procedure, the animals received an intraperitoneal injection of analgesics and antibiotics [5 mg/kg Baytril (Bayer) and 2.5 mg/kg Finadyne (Essex)]. The animals to be left for 48 h received another injection of analgesics and antibiotics after 24 h.

In Vivo MRI Experiments. For the MRI experiments, the animals were anesthetized with 1.5−2% isoflurane and placed in a homemade quadrature coil integrated within a stereotaxic animal holder. The head holder was adapted with movable bite and ear bars and positioned fixed on a magnet chair. This allowed precise positioning of the animal with respect to the coil and the magnet, avoiding movement artifacts. Body temperature, heart rate, CO_2, and SpO_2 were monitored throughout the scanning session. Two to three scanning sessions were performed with each animal. We typically scanned the animals before, immediately after, and 24−48 h after the injection of CAs. One scan session for an individual animal consisted of five to seven scans of 18 min each.

Experiments were carried out in a vertical 7T (300 MHz)/60 cm diameter bore magnet (Bruker BioSpin, Ettlingen, Germany). The saddle coil, which was designed to generate a homogeneous field over the whole rat brain, was used to transmit and receive. The MR system was controlled via a Bruker BioSpec console (ParaVision 3, 4, and 5 at different time periods) running under the Linux operating system. We used a modified driven equilibrium Fourier transform (MDEFT) method with MDEFT preparation[40] to obtain T_1-weighted anatomical images. The scan parameters were: TR = 22.2 ms, TE = 4.8 ms, FA = 20°, ID = 1000 ms and four segments. The geometric parameters of the 3D scans were matrix $192 \times 136 \times 100$, FOV = $48 \times 34 \times 25$ mm^3, and voxel size $0.25 \times 0.25 \times 0.25$ mm^3.

The MRI images were analyzed with custom-developed Matlab functions (v7.5.0, MathWorks). An automated realignment procedure of SPM (statistical parametric mapping, www.fil.ion.ucl.ac.uk) was applied to coregister all scans. For statistical analysis, the image intensity was normalized to reference signal intensity in the head muscles. Statistical maps were generated by implementing a Student's t test (unpaired) at each voxel comparing brain images before and 24−48 h after CAs injection. The significant voxels represent the pattern of T_1-weighted MRI signal enhancement induced by the neuronal transport of CAs. The arbitrary significance threshold was set to $P < 0.01$ (uncorrected for multiple comparisons) for individual voxels, and a minimum cluster size of three contiguous voxels constituting at least 3% of the total number of voxels for a given region of interest (ROI). The same data were also tested for lower or higher p-values.

Perfusion. After the last MRI session, the animals received a lethal intraperitoneal injection of the barbiturate pentobarbital sodium (Narcoren from Merial; 2.5 mL/kg body weight). After cessation of all reflexes, the chest of the animal was opened and 0.4 mL of Heparin-Sodium 25000 (ratiopharm) was injected into the heart in order to prevent coagulation. Then a cannula was inserted and the animal was perfused with isotonic saline (using NaCl 0.9 E from Fresenius) for about 5 min and then with the fixative (commercially available 4% paraformaldehyde, phosphate buffered; Roti-Histofix 4% from Carl Roth). The brain was removed from the skull and kept in the fixative overnight. On the next day, the brain was transferred into 30% sucrose in demineralized water and kept there for at least 4 days until it had sunk. The brain was then sliced into serial sections with a cryotome at a thickness of 70 μm.

Histological Procedure. The protocol largely followed that of Horikawa and Armstrong[41] with some modifications suggested by Dr. Michaela Schweizer (personal communication). In detail, the sections were collected in phosphate buffer (PB, 0.1 M; pH 7.3), rinsed again in PB, and then transferred into 1% H_2O_2 in PB for 1 h, in order to block endogenous peroxidase activity. After rinsing three times in PB, the sections were kept for 1 h and 30 min in Triton X-100 (2% in 0.1 M PB from Carl Roth). They were then incubated overnight in avidin-conjugated peroxidase (ABC Elite PK 6100 from Linaris, 1% in 0.1 M PB: i.e., adding 10 drops (50 μL each) of each of the two solutions to 49 mL of buffer; note that the ABC mixture must stand for 30 min before use). On the next day, the sections were rinsed 2 × 10 min in PB (0.1 M) and then 2 × 10 min in Tris/HCl at pH 7.9 (using a 0.1 M solution of tris(hydroxymethyl)aminomethane and pH adjusted to 7.9 with HCl; we usually used a 1 M stock solution, the pH of which we adjusted with concentrated HCl). The sections were then transferred into a solution of diaminobenzidine (DAB) and H_2O_2 (DAB tablets were dissolved in demineralized water) for 30−45 min. After washing three times in Tris/HCl, the sections were transferred into 0.05 M PB and mounted on electrostatic slides (Superfrost Plus, Menzel, ThermoScientific), air-dried overnight, dehydrated in ethanol (70%, 2 × 99%, 1 × 100% ethanol, 2 × terpineole, and 2 × xylene), and covered in Eukitt or DePeX.

■ ASSOCIATED CONTENT

Supporting Information. ^{1}H NMR of **L**, ESI-MS spectra of **L**/[**Gd.L**], Figure S1 (viability for 24 h incubation), and HPLC chromatogram of [**Gd.L**]. This material is available free of charge via Internet at http://pubs.acs.org.

■ AUTHOR INFORMATION

Corresponding Author

*(A.M.) Mailing address: Department of Chemistry, Durham University, South Road, Durham DH1 3LE, England. E-mail: anurag.mishra@durham.ac.uk. (S.C.) Mailing address: Instituto de Neurociencias CSIC-UMH, 03550 San Juan de Alicante, Spain. E-mail: scanals@umh.es.

Present Addresses

$^{\perp}$Department of Chemistry, Durham University, South Road, Durham DH1 3LE, England.

Author Contributions

A.M. and S.C. conceived the Project. A.M. performed the chemical synthesis. A.M. and J.E. did the in vitro characterization of the CA. M.B. and S.C. did the MRI experiments and analyzed the data. A.M. and A.S. performed the histological characterization of the CA. N.K.L. supported the research. All authors wrote the paper.

Funding Sources

This work was supported by the Max-Planck Society and the Hertie Foundation. S.C. acknowledges the support of the Human Frontiers Science Program Organization and the Ministry of Science and Innovation of Spain (BFU2009-09938) and the Consolider-Ingenio 2010 Program (CSD2007-0023). A.M. acknowledges the support of the EC for a Marie Curie IEF (PIEF-GA-2009-237253).

■ ACKNOWLEDGMENT

The authors thank Dr. Henry Evrard, for his help in making pressure injections, Dr. Ritu Mishra for her excellent help with the cell culture experiments and Prof. Bernd Hamprecht, for the kind gift of the N18 mouse neuroblastoma cell line.

■ REFERENCES

(1) Arenkiel, B. R., and Ehlers, M. D. (2009) Molecular genetics and imaging technologies for circuit-based neuroanatomy. *Nature 461*, 900–907.

(2) Robinson, T. E., and Kolb, B. (2004) Structural plasticity associated with exposure to drugs of abuse. *Neuropharmacology 47* (Suppl 1), 33–46.

(3) Braitenberg, V., and Schüz, A. (1998) *Statistics and Geometry of Neuronal Connectivity*, Springer, Berlin, Heidelberg.

(4) Destexhe, A., and Marder, E. (2004) Plasticity in single neuron and circuit computations. *Nature 431*, 789–795.

(5) Palop, J. J., Chin, J., and Mucke, L. (2006) A network dysfunction perspective on neurodegenerative diseases. *Nature 443*, 768–773.

(6) Canals, S., Beyerlein, M., Merkle, H., and Logothetis, N. K. (2009) Functional MRI evidence for LTP-induced neural network reorganization. *Curr. Biol. 19*, 398–403.

(7) Kobbert, C., Apps, R., Bechmann, I., Lanciego, J. L., Mey, J., and Thanos, S. (2000) Current concepts in neuroanatomical tracing. *Prog. Neurobiol. 62*, 327–351.

(8) Pautler, R. G., Silva, A. C., and Koretsky, A. P. (1998) In vivo neuronal tract tracing using manganese-enhanced magnetic resonance imaging. *Magn. Reson. Med. 40*, 740–748.

(9) Canals, S., Beyerlein, M., Keller, A. L., Murayama, Y., and Logothetis, N. K. (2008) Magnetic resonance imaging of cortical connectivity in vivo. *Neuroimage 40*, 458–472.

(10) Leergaard, T. B., Bjaalie, J. G., Devor, A., Wald, L. L., and Dale, A. M. (2003) In vivo tracing of major rat brain pathways using manganese-enhanced magnetic resonance imaging and three-dimensional digital atlasing. *Neuroimage 20*, 1591–1600.

(11) Saleem, K. S., Pauls, J. M., Augath, M., Trinath, T., Prause, B. A., Hashikawa, T., and Logothetis, N. K. (2002) Magnetic resonance imaging of neuronal connections in the macaque monkey. *Neuron 34*, 685–700.

(12) Van der Linden, A., Verhoye, M., Van Meir, V., Tindemans, I., Eens, M., Absil, P., and Balthazart, J. (2002) In vivo manganese-enhanced magnetic resonance imaging reveals connections and functional properties of the songbird vocal control system. *Neuroscience 112*, 467–474.

(13) Murayama, Y., Weber, B., Saleem, K. S., Augath, M., and Logothetis, N. K. (2006) Tracing neural circuits in vivo with Mn-enhanced MRI. *Magn. Reson. Imaging 24*, 349–358.

(14) Watanabe, T., Frahm, J., and Michaelis, T. (2004) Functional mapping of neural pathways in rodent brain in vivo using manganese-enhanced three-dimensional magnetic resonance imaging. *NMR Biomed. 17*, 554–568.

(15) Pautler, R. G., Mongeau, R., and Jacobs, R. E. (2003) In vivo trans-synaptic tract tracing from the murine striatum and amygdala utilizing manganese enhanced MRI (MEMRI). *Magn. Reson. Med. 50*, 33–39.

(16) Chandra, S. V., Shukla, G. S., Srivastava, R. S., Singh, H., and Gupta, V. P. (1981) An exploratory study of manganese exposure to welders. *Clin Toxicol. 18*, 407–416.

(17) McMillan, D. E. (1999) A brief history of the neurobehavioral toxicity of manganese: some unanswered questions. *Neurotoxicology 20*, 499–507.

(18) Bock, N. A., Paiva, F. F., and Silva, A. C. (2008) Fractionated manganese-enhanced MRI. *NMR Biomed. 21*, 473–478.

(19) Eschenko, O., Canals, S., Simanova, I., and Logothetis, N. K. (2010) Behavioral, electrophysiological and histopathological consequences of systemic manganese administration in MEMRI. *Magn. Reson. Imaging 28*, 1165–1174.

(20) Eschenko, O., Canals, S., Simanova, I., Beyerlein, M., Murayama, Y., and Logothetis, N. K. (2010) Mapping of functional brain activity in freely behaving rats during voluntary running using manganese-enhanced MRI: implication for longitudinal studies. *Neuroimage 49*, 2544–2555.

(21) King, M. A., Louis, P. M., Hunter, B. E., and Walker, D. W. (1989) Biocytin: a versatile anterograde neuroanatomical tract-tracing alternative. *Brain Res. 497*, 361–367.

(22) Mishra, A., Pfeuffer, J., Mishra, R., Engelmann, J., Mishra, A. K., Ugurbil, K., and Logothetis, N. K. (2006) A new class of Gd-based DO3A-ethylamine-derived targeted contrast agents for MR and optical imaging. *Bioconjugate Chem. 17*, 773–780.

(23) Mishra, A., Fouskova, P., Angelovski, G., Balogh, E., Mishra, A. K., Logothetis, N. K., and Toth, E. (2008) Facile Synthesis and Relaxation Properties of Novel Bispolyazamacrocyclic Gd(3+) Complexes: An Attempt towards Calcium-Sensitive MRI Contrast Agents. *Inorg. Chem. 47*, 3460.

(24) Mishra, A., Logothetis, N. K., and Parker, D. (2011) Critical In Vitro Evaluation of Responsive MRI Contrast Agents for Calcium and Zinc. *Chem.—Eur. J. 17* (5), 1529.

(25) Congreve, A., Parker, D., Gianolio, E., and Botta, M. (2004) Steric control of lanthanide hydration state: fast water exchange at gadolinium in a mono-amide 'DOTA' complex. *Dalton Trans.* 1441–1445.

(26) Caravan, P., Ellison, J. J., McMurry, T. J., and Lauffer, R. B. (1999) Gadolinium(III) Chelates as MRI Contrast Agents: Structure, Dynamics, and Applications. *Chem. Rev. 99*, 2293–2352.

(27) Botta, M. (2000) Second coordination sphere water molecules and relaxivity of gadolinium(III) complexes: Implications for MRI contrast agents. *Eur. J. Inorg. Chem.* 399–407.

(28) Aime, S., Botta, M., Parker, D., and Williams, J. A. G. (1996) Extent of hydration of octadentate lanthanide complexes incorporating phosphinate donors: Solution relaxometry and luminescence studies. *J. Chem. Soc., Dalton Trans.* 17–23.

(29) Wilchek, M., and Bayer, E. A. (1990) Biotin-containing reagents. *Methods Enzymol. 184*, 123–138.

(30) Livramento, J. B., Weidensteiner, C., Prata, M. I., Allegrini, P. R., Geraldes, C. F., Helm, L., Kneuer, R., Merbach, A. E., Santos, A. C., Schmidt, P., and Toth, E. (2006) First in vivo MRI assessment of a self-assembled metallostar compound endowed with a remarkable high field relaxivity. *Contrast Media Mol. Imaging 1*, 30–39.

(31) Rohrer, M., Bauer, H., Mintorovitch, J., Requardt, M., and Weinmann, H. J. (2005) Comparison of magnetic properties of MRI contrast media solutions at different magnetic field strengths. *Invest. Radiol. 40*, 715–724.

(32) Caravan, P., Farrar, C. T., Frullano, L., and Uppal, R. (2009) Influence of molecular parameters and increasing magnetic field strength on relaxivity of gadolinium- and manganese-based T-1 contrast agents. *Contrast Media Mol. Imaging 4*, 89–100.

(33) Marchisio, P. C., Weber, K., and Osborn, M. (1979) Identification of multiple microtubule initiating sites in mouse neuroblastoma cells. *Eur. J. Cell Biol. 20*, 45–50.

(34) Rennert, R., Wespe, C., Beck-Sickinger, A. G., and Neundorf, I. (2006) Developing novel hCT derived cell-penetrating peptides with improved metabolic stability. *Biochim. Biophys. Acta 1758*, 347–354.

(35) Paxinos, G., Watson, C. (2007) The rat brain in stereotaxic coordinates, 6 ed.; Academic Press: Elsevier, Oxford, UK.

(36) Baur, B., Suormala, T., and Baumgartner, E. R. (2002) Biocytin and biotin uptake into NB2a neuroblastoma and C6 astrocytoma cells. *Brain Res. 925*, 111–121.

(37) Richards, W. L., Song, M. K., Krutzsch, H., Evarts, R. P., Marsden, E., and Thorgeirsson, S. S. (1985) Measurement of cell proliferation in microculture using Hoechst 33342 for the rapid semi-automated microfluorimetric determination of chromatin DNA. *Exp. Cell Res. 159*, 235–246.

(38) Blaheta, R. A., Franz, M., Auth, M. K., Wenisch, H. J., and Markus, B. H. (1991) A rapid non-radioactive fluorescence assay for the measurement of both cell number and proliferation. *J. Immunol. Methods 142*, 199–206.

(39) Mishra A., Dhingra. K., Mishra R., Schüz, A., Engelmann J., Beyerline M., Canals S., and Logothetis N. K. (2011) Biocytin-based Contrast Agents for Molecular Imaging: An Approach to Developing New In Vivo Neuroanatomical Tracers for MRI. In *Neuroimage*, InTech, Rijeka, Croatia, ISBN 978-953-307-413-9, in press.

(40) Lee, J. H., Garwood, M., Menon, R., Adriany, G., Andersen, P., Truwit, C. L., and Ugurbil, K. (1995) High contrast and fast three-dimensional magnetic resonance imaging at high fields. *Magn. Reson. Med. 34*, 308–312.

(41) Horikawa, K., and Armstrong, W. E. (1988) A versatile means of intracellular labeling: injection of biocytin and its detection with avidin conjugates. *J. Neurosci. Methods 25*, 1–11.